A strains of the H1N1 subtype replicate efficiently in mice only after they are adapted to growth in these animals (*21*). The MID_{50} titers, determined through the detection of virus in the lungs of mice 3 days after inoculation, were markedly low (MID_{50} = $10^{0.5–1.5}$ PFU or EID_{50}), indicating high infectivity in this model. We next determined whether 2009 A(H1N1) influenza viruses replicated systemically in the mouse after intranasal infection, a characteristic of virulent avian influenza (H5N1) viruses isolated from humans but not of 1918 (H1N1) virus (*17*, *22*). All mice infected with CA/04, TX/15, or MX/4108 viruses had undetectable levels (<10 PFU/ml) of virus in whole spleen, thymus, brain, and intestinal tissues, indicating that the 2009 A(H1N1) influenza viruses did not spread to extrapulmonary organs in the mouse.

The full clinical spectrum of disease caused by 2009 A(H1N1) influenza viruses and its transmissibility are not completely understood. The present study shows that overall morbidity and lung viral titers were higher in ferrets infected with 2009 A(H1N1) influenza virus isolates as compared with those infected with the seasonal H1N1 virus. Moreover, the detection of 2009 A(H1N1) influenza viruses in the intestinal tissue of ferrets is consistent with gastrointestinal involvement among some human 2009 A(H1N1) cases (*6*). Although the 2009 A(H1N1) influenza viruses demonstrated similar replication kinetics as the seasonal H1N1 virus in the upper respiratory tract of inoculated ferrets, the 2009 A(H1N1) influenza viruses did not spread to all naïve ferrets by means of respiratory droplets. This lack of efficient respiratory droplet transmission suggests that additional virus adaptation in mammals may be required to reach the high-transmissible phenotypes observed with seasonal H1N1 or the 1918 pandemic virus (*14*, *17*).

It was demonstrated previously (*17*) that the efficiency of respiratory droplet transmission in ferrets correlates with the α2-6–binding affinity of the viral HA. In fact, a single amino acid mutation in HA of the efficiently transmitting SC18 virus led to a virus (NY18) that transmitted inefficiently (fig. S5). The α2-6–binding affinity of NY18 HA was substantially lower than that of SC18 HA (fig. S5). In a similar fashion, the substantially lower α2-6–binding affinity of CA/04 HA than that of SC18 HA correlates with the less efficient 2009 A(H1N1) influenza virus respiratory droplet transmission (fig. S5).

Adaptation of the polymerase basic protein 2 (PB2) is also critical for efficient aerosolized respiratory transmission of an H1N1 influenza virus (*14*, *17*, *23*). A single amino acid substitution from glutamic acid to lysine at amino acid position 627 supports efficient influenza virus replication at the lower temperature (33°C) found in the mammalian airway and contributes to efficient transmission in mammals (*14*, *23*). All three of the 20th-century influenza pandemics were caused by viruses containing human adapted PB2 genes, and in general lysine is present at position 627 among the human influenza viruses, whereas a glutamic acid is found in this position among the avian influenza isolates that fail to transmit efficiently among ferrets (*14*). In contrast to the Brisbane/07 virus and other seasonal H1N1 viruses, all 2009 A(H1N1) influenza viruses to date with an avian influenza lineage PB2 gene possess a glutamic acid at residue 627 (*1*). The phenotype of PB2 is determined by the amino acid at position 627, which can arise by mutant selection or reassortment, and along with adaptive changes in the RBS should be closely monitored as markers for enhanced virus transmission.

References and Notes

1. R. J. Garten *et al.*, *Science* **325**, 5937 (2009); published online 22 May 2009 (10.1126/science.1176225).
2. *MMWR Morb. Mortal. Wkly. Rep.* **58**, 453 (2009).
3. *MMWR Morb. Mortal. Wkly. Rep.* **58**, 400 (2009).
4. *MMWR Morb. Mortal. Wkly. Rep.* **58**, 467 (2009).
5. http://www.who.int/en/
6. F. S. Dawood *et al.*, *J. Med.* **360**, 2605 (2009).
7. C. Fraser *et al.*, *Science* **324**, 1557 (2009); published online 11 May 2009 (10.1126/science.1176062).
8. T. M. Tumpey, J. A. Belser, *Annu. Rev. Microbiol.* **63**, 252 (2009).
9. R. J. Webby, R. G. Webster, *Science* **302**, 1519 (2003).
10. C. Viboud *et al.*, *Vaccine* **24**, 6701 (2006).
11. T. R. Maines *et al.*, *Proc. Natl. Acad. Sci. U.S.A.* **103**, 12121 (2006).
12. J. A. Belser *et al.*, *Proc. Natl. Acad. Sci. U.S.A.* **105**, 7558 (2008).
13. A. C. Lowen, P. Palese, *Infect. Disord. Drug Targets* **7**, 318 (2007).
14. N. Van Hoeven *et al.*, *Proc. Natl. Acad. Sci. U.S.A.* **106**, 3366 (2009).
15. Materials and methods are available as supporting material on *Science* Online.
16. H. L. Yen *et al.*, *J. Virol.* **81**, 6890 (2007).
17. T. M. Tumpey *et al.*, *Science* **315**, 655 (2007).
18. A. Srinivasan *et al.*, *Proc. Natl. Acad. Sci. U.S.A.* **105**, 2800 (2008).
19. A. Chandrasekaran *et al.*, *Nat. Biotechnol.* **26**, 107 (2008).
20. V. Soundararajan *et al.*, *Nat. Biotechnol.* **27**, 510 (2009).
21. C. A. Hartley, P. C. Reading, A. C. Ward, E. M. Anders, *Arch. Virol.* **142**, 75 (1997).
22. T. R. Maines *et al.*, *J. Virol.* **79**, 11788 (2005).
23. J. Steel, A. C. Lowen, S. Mubareka, P. Palese, *PLoS Pathog.* **5**, e1000252 (2009).

24. We thank P. Blair (Naval Health Research Center, San Diego), G. J. Demmler (Texas Children's Hospital, Houston), C. Alpuche-Aranda [Instituto de Diagnóstico y Referencia Epidemiológicos, Mexico], and the WHO Collaborating Centre for Reference and Research on Influenza (Melbourne) for facilitating access to viruses. We also thank X. Lu and A. Balish for preparation of viruses and V. Veguilla for statistical analysis. R.S. acknowledges the consortium for functional glycomics for providing glycan standards and support from the Singapore-MIT Alliance for Research and Technology and the National Institute of General Medical Sciences of the NIH (GM 57073 andU54 GM62116). Confocal microscopy of the human lung tissue sections was performed at the W. M. Keck Foundation Biological Imaging Facility at the Whitehead Institute. The findings and conclusions in this report are those of the authors and do not necessarily reflect the views of the funding agency.

Supporting Online Material

www.sciencemag.org/cgi/content/full/1177238/DC1
Materials and Methods
Figs. S1 to S5
Table S1
References

3 June 2009; accepted 23 June 2009
Published online 2 July 2009;
10.1126/science.1177238
Include this information when citing this paper.

Chlamydomonas Swims with Two "Gears" in a Eukaryotic Version of Run-and-Tumble Locomotion

Marco Polin,[1] Idan Tuval,[1] Knut Drescher,[1] J. P. Gollub,[1,2] Raymond E. Goldstein[1]*

The coordination of eukaryotic flagella is essential for many of the most basic processes of life (motility, sensing, and development), yet its emergence and regulation and its connection to locomotion are poorly understood. Previous studies show that the unicellular alga *Chlamydomonas*, widely regarded as an ideal system in which to study flagellar biology, swims forward by the synchronous action of its two flagella. Using high-speed imaging over long intervals, we found a richer behavior: A cell swimming in the dark stochastically switches between synchronous and asynchronous flagellar beating. Three-dimensional tracking shows that these regimes lead, respectively, to nearly straight swimming and to abrupt large reorientations, which yield a eukaryotic version of the "run-and-tumble" motion of peritrichously flagellated bacteria.

One of the most highly conserved structures among eukaryotes is the flagellum (*1*, *2*), whose composition in humans is nearly identical to that in unicellular algae (*3*). Because the coordinated motion of flagella is involved in fluid transport in the respiratory system (*4*), embryonic left-right asymmetry (*5*, *6*), intercellular communication (*7*), and possibly the evolution of multicellularity (*8*), it is important to understand the origin of flagellar synchronization. An emerging hypothesis (*9*–*12*) implicates hydrodynamic interactions, yet experimental proof is lacking. Flagellar synchronization is also important for prokaryotes, in which "run-and-tumble"

[1]Department of Applied Mathematics and Theoretical Physics, University of Cambridge, Wilberforce Road, Cambridge CB3 0WA, UK. [2]Department of Physics, Haverford College, Haverford, PA 19041, USA.

*To whom correspondence should be addressed. E-mail: R.E.Goldstein@damtp.cam.ac.uk

chemotaxis relies on the stochastic bundling and unbundling of flagella (*13*), resulting in individual random walks and the diffusion of populations (*14*).

Here, we ask whether eukaryotic locomotion has any relationship to the run-and-tumble paradigm, using the alga *Chlamydomonas reinhardtii* as a model (*15*, *16*). Its two flagella are termed cis and trans because of their positions relative to the eyespot, a rudimentary light-sensing organelle. Analysis of cells in the dark, over short (1- to 2-s) intervals (*17*, *18*), has shown two behaviors. Most cells (~95%) beat with a synchronous breaststroke interrupted occasionally by extra beats ("slips") of the trans flagellum, a phenomenon confirmed by later experiments over much longer periods (*19*). In this regime, cells swim in a tight helix along an almost straight center line. The remaining cells (~5%) beat asynchronously, with a large interflagellar frequency difference (10 to 30%), compatible with observations on demembranated cells (*20*), where trans flagella often beat with a higher frequency than cis flagella. These results have been interpreted as representative of distinct subpopulations. However, the underlying biochemical or physical processes that control synchronization remain unknown.

Previous studies tracking *C. reinhardtii* swimming (*21*–*23*) suggest that, like bacteria, entire populations display diffusive behavior. Existing interpretations (*22*) attribute diffusion to the accumulation of small deflections but lack explicit references to the actual beating dynamics of the flagella.

Here, we present three main experimental results on the beating of *C. reinhardtii* flagella and its relationship to swimming in the dark, where phototactic reorientations do not occur. First, we demonstrate that individual cells stochastically switch over the course of time between the two regimes: synchronous with slips and asynchronous. Second, we show that either the cis or the trans flagellum can be the faster one during asynchrony, so although their phototactic responses are intrinsically different (*17*, *18*, *20*), there is no absolute frequency asymmetry. Third, we present strong evidence that the diffusion of populations of *C. reinhardtii* is the result of localized events of large nonphototactic reorientations, corresponding to periods of asynchronous flagellar beating. Taken together, these results strongly suggest that the beating frequencies themselves are under the control of the cell. The stochastic movement back and forth between synchrony and asynchrony is reminiscent of the run-and-tumble motion of bacteria, with sharp turns taking the place of tumbles.

We first studied (*24*) the diffusion of a population of *C. reinhardtii* by gently centrifuging a dilute suspension of cells to the bottom of a plastic cuvette and analyzing the dynamics of the concentration profile as it spread upward (Fig. 1, A and B). In a region far from the bottom of the chamber, where cell-cell interactions are rare, the concentration flux is a linear function of the concentration gradient (Fig. 1C), and the slope of the fitted line gives then an estimate of the diffusion constant for an isolated individual: $D_{exp} = (0.68 \pm 0.11) \times 10^{-3}$ cm^2/s. A random walk of typical speed u and free-flight time τ gives a diffusion constant $D \sim u^2\tau$, implying a characteristic time on the order of 5 to 10 s for $u \sim 100$ μm/s.

To interpret this time and connect the macroscopic diffusive behavior to the dynamics of individual cells, we analyzed in a separate experiment high-speed movies of the flagella pairs of isolated *C. reinhardtii* cells held by micropipettes. The fact that a given cell moves back and forth between synchronous and asynchronous states is illustrated in Fig. 2. Figure 2A shows time series of the individual signals from the left and right flagella over a short (0.5-s) interval within a period of synchrony several seconds long, whereas Fig. 2B displays the asynchronous state in which the interflagellar phase difference drifts linearly in time

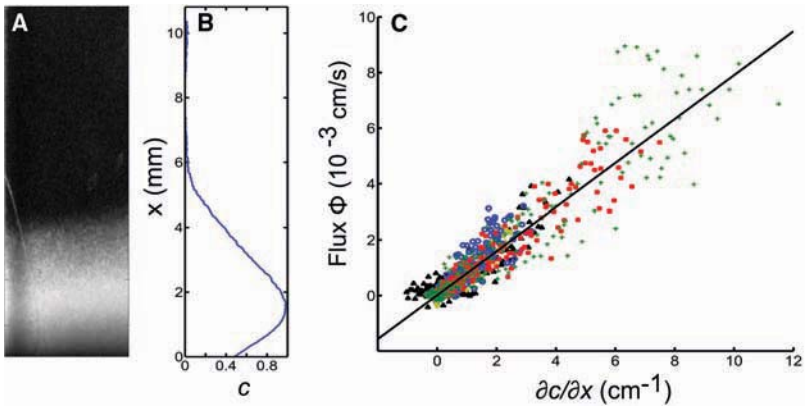

Fig. 1. Diffusive behavior of a population of *C. reinhardtii* containing thousands of individual cells. (**A**) Light scattered from the cells 1 min after being spun in a centrifuge. (**B**) Integrated light intensity as a function of height x. (**C**) Flux versus concentration gradient at various points in space and time; the linearity shows that cells spread according to Fick's law. Different-colored symbols correspond to independent trials.

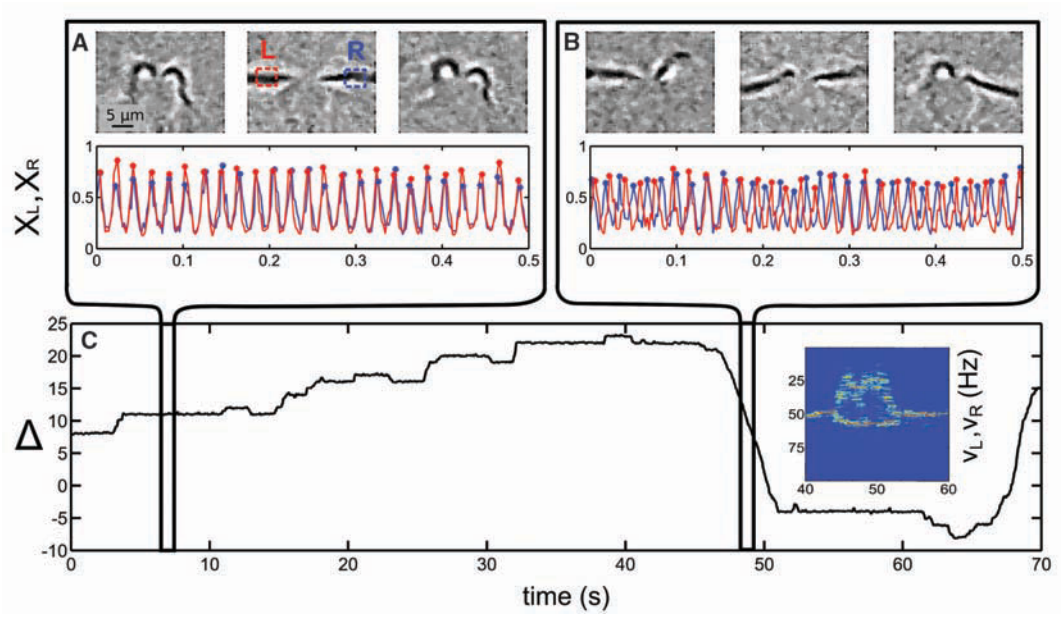

Fig. 2. A single *C. reinhardtii* cell moves back and forth between synchronous (**A**) and asynchronous (**B**) states. Movie frames showing a few cycles and the oscillatory intensity signals $X_{L,R}(t) = \Gamma_{L,R}(t)\sin[2\pi\theta_{L,R}(t)]$ (X, signal; L, left; R, right; Γ, amplitude; t, time; θ, phase), obtained by local sampling of the video light intensity near the two flagella, are shown for both cases. (**C**) A long (70-s) time series of the phase difference $\Delta(t) = \theta_L(t) - \theta_R(t)$ contains periods of synchrony interrupted by drifts of either sign. A windowed Fourier transform of the beating signals during the transition from synchronization to drifting and then back again to synchrony (inset) shows a large frequency difference in the asynchronous state. This behavior was characteristic of all 24 observed cells.

over tens of cycles. These short intervals are part of a much longer measurement window of 70 s (Fig. 2C). In this long time series, we see that drifts extend over periods of 1 to 3 s and can be of either sign. The interflagellar frequency difference during drifts is in the range from 10 to 30% of the mean (inset Fig. 2C). Synchronous intervals are more frequently interrupted by much shorter events (~0.2 s) resulting in a single extra beat of one flagellum: a phase slip. Slips can be of either sign, but are biased in one direction, constant throughout each experiment, and happen randomly in time. This behavior was characteristic of all the observed cells (*24*).

On a basic level, the two flagella of *C. reinhardtii* are oscillators, coupled through the fluid in which they move and possibly the cell wall through which they emerge, and subject to noise of both thermal and biochemical origin. Despite their complexity, the basic phenomenology can be captured by a simple mathematical model describing the dynamics of weakly coupled self-sustained noisy oscillators (*24*, *25*). Three parameters characterize this model: the interflagellar coupling strength ε, the flagellar noise intensity T_{eff}, and the intrinsic frequency difference between the two flagella $\delta\nu$, which can be determined even in the synchronized state and is responsible for the bias in the distribution of slips. The distribution of the measured coupling strengths ε (Fig. 3A) shows a well-defined peak at a value that compares very well with a rough estimate ε_m given by an idealized flagellar model with hydrodynamic coupling (*24*). This suggests that fluid flow is indeed the major contribution to the coupling responsible for flagellar synchronization.

Synchronous and asynchronous states cluster into two regions in parameter space, separated by nearly two orders of magnitude in the intrinsic interflagellar frequency difference (Fig. 3B), with no cells at intermediate values. These two distinct dynamical regimes are analogous to two distinct internal "gears." In the lower gear (a lower value of $\delta\nu$), the intrinsic interflagellar frequency difference is sufficiently small for the coupling to lead to robust synchronization. In the upper gear, the flagella beat with a high intrinsic frequency difference, and the coupling is too weak to cause significant frequency entrainment. Because individual cells alternate in time between these two regimes, we conclude that *C. reinhardtii* can control the state of synchronization of its flagella by actively changing their intrinsic frequency difference.

The stochastic switching between synchrony and asynchrony has clear effects on swimming trajectories. Figure 4A shows a portion of the

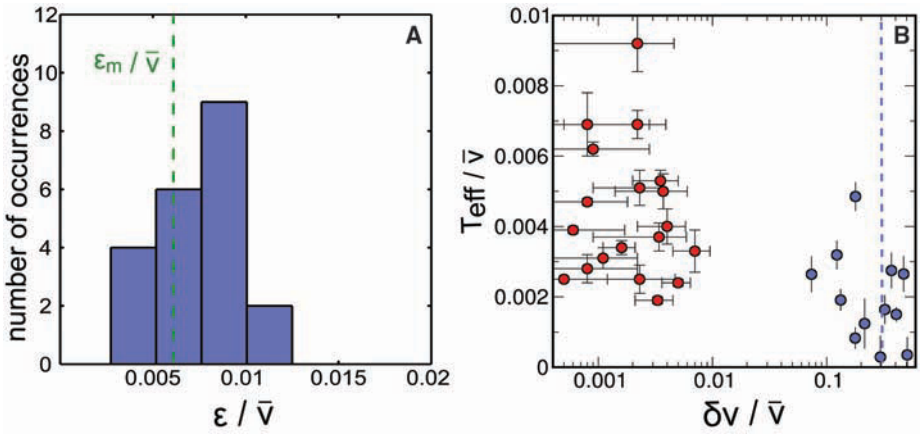

Fig. 3. Parameters of the phase synchronization model (*24*) extracted from high-speed imaging studies of flagellar dynamics, rescaled by the mean flagellar beating frequency $\bar{\upsilon}$. (**A**) The probability distribution of the coupling amplitude $\varepsilon/\bar{\upsilon}$ shows a well-defined peak at 0.0076, comparable to the estimate $\varepsilon_m/\bar{\upsilon}$ = 0.006 based on hydrodynamic interactions. (**B**) Data clustering in the parameter space defined by the intrinsic interflagellar frequency difference $\delta\nu$ and the flagellar noise intensity T_{eff} supports the existence of two distinct regimes. Although the noise differences are modest, the relative intrinsic frequency differences span two orders of magnitude, from 0.001–0.01 to 0.1–0.4. The dashed vertical line represents the intrinsic frequency difference observed in cell models (*20*).

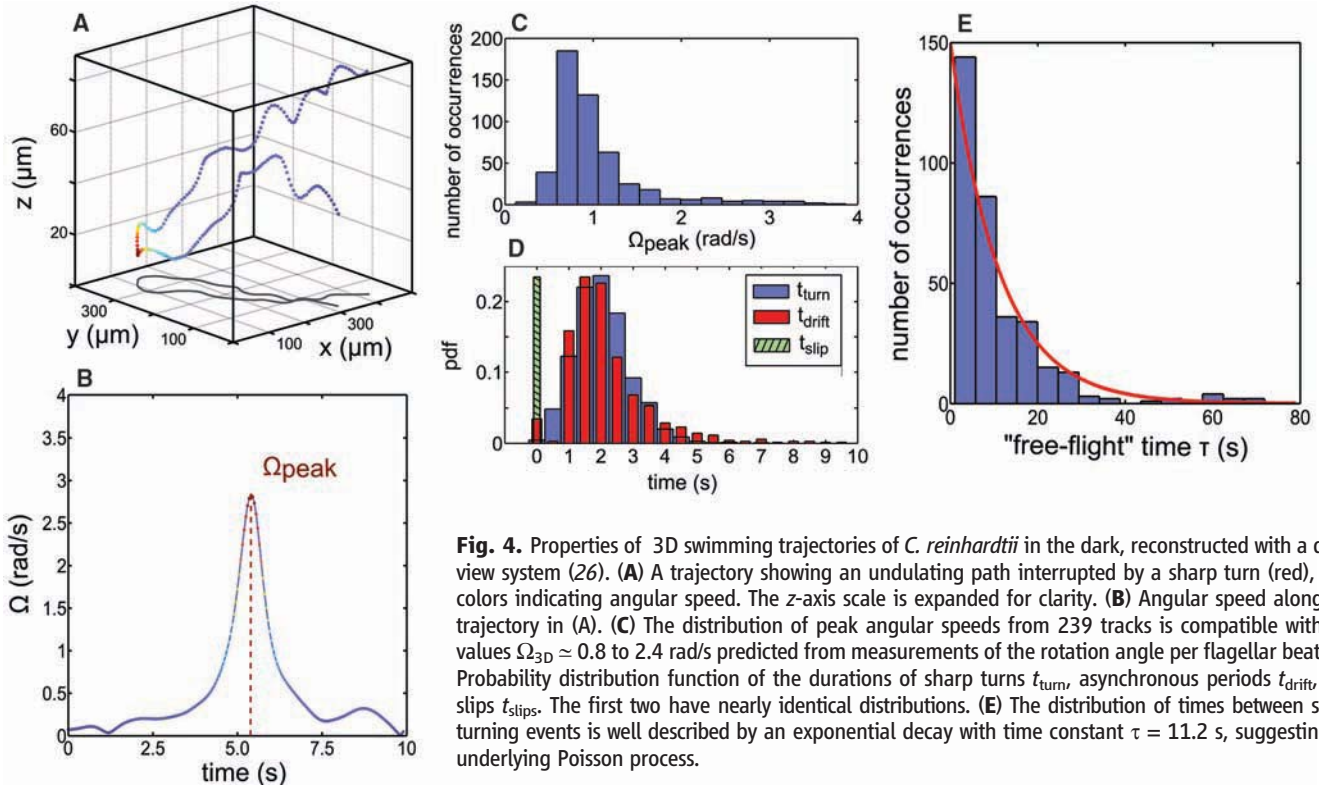

Fig. 4. Properties of 3D swimming trajectories of *C. reinhardtii* in the dark, reconstructed with a dual-view system (*26*). (**A**) A trajectory showing an undulating path interrupted by a sharp turn (red), with colors indicating angular speed. The *z*-axis scale is expanded for clarity. (**B**) Angular speed along the trajectory in (A). (**C**) The distribution of peak angular speeds from 239 tracks is compatible with the values $\Omega_{3D} \simeq 0.8$ to 2.4 rad/s predicted from measurements of the rotation angle per flagellar beat. (**D**) Probability distribution function of the durations of sharp turns t_{turn}, asynchronous periods t_{drift}, and slips t_{slips}. The first two have nearly identical distributions. (**E**) The distribution of times between sharp turning events is well described by an exponential decay with time constant τ = 11.2 s, suggesting an underlying Poisson process.

three-dimensional (3D) reconstruction (*26*) of a trajectory containing both helical swimming and a clearly recognizable sharp turning event (Fig. 4B). Analysis of hundreds of sharp turns from 3D trajectories (*24*) yields the probability distribution of their angular speeds (Fig. 4C) and duration (Fig. 4D). The range of angular speeds is consistent with an estimate derived from the average frequency difference during asynchronous beating periods and the average angular rotation of the cell body per flagellar beat (*24*). The distribution of durations of turns is nearly identical to that of drifts (Fig. 4D) and incompatible with that of slips, the only other observed behavior that could lead to turns in the dark. These results indicate that sharp turns are the direct consequence of periods of asynchronous flagellar beating. Because sharp turns are defined by angular speeds much higher than typical background rates (Fig. 4B), we choose to consider these as the only turning events, which separate straight-line free-flight segments. The probability distribution of the duration of such free flights, shown in Fig. 4E, decays exponentially with a mean of $\tau = 11.2$ s. This time scale is clearly the one inferred earlier from the macroscopic diffusion measurements. The diffusion constant D can be estimated more precisely with the well-known results from run-and-tumble random walk models (*14*). With the average parameters extracted from the 3D trajectories, we obtain (*24*) $D \cong (0.47 \pm 0.05) \times 10^{-3}$ cm^2/s, which is in very good agreement with the value estimated from the macroscopic measurements on large populations.

We have found that in the dark, *C. reinhardtii* can vary the intrinsic frequencies of its two flagella so that they alternate between synchronous and asynchronous beating, with synchrony realized though a mechanism consistent with hydrodynamic coupling. This leads to swimming trajectories with stochastically distributed sharp turns and ultimately to the diffusive behavior of a population. In contrast to previous observations on cell models (*20*), we showed that in each cell either flagellum can beat faster than the other. This approximate symmetry is a strong indication that the unknown regulatory system at work here is distinct from that governing phototaxis, which is based instead on opposite amplitude modulations of flagellar motion, and it shows that the idea of a well-defined intrinsic frequency difference between cis and trans flagella is incorrect. Such control mechanisms could also have a role in coordinating large numbers of cilia in simple multicellular organisms lacking a central nervous system (such as *Volvox*). Open issues include the origins of this regulation, the characteristic time scale between asynchronous intervals, and the noise of flagellar beats, along with the possible interplay of these processes with chemotaxis and phototaxis.

References and Notes

1. I. Ibañez-Tallon, N. Heintz, H. Omran, *Hum. Mol. Genet.* **12**, R27 (2003).
2. G. J. Pazour, N. Agrin, J. Leszyk, G. B. Witman, *J. Cell Biol.* **170**, 103 (2005).
3. D. R. Mitchell, *J. Phycol.* **36**, 261 (2000).
4. B. A. Afzelius, *Science* **193**, 317 (1976).
5. S. Nonaka *et al.*, *Cell* **95**, 829 (1998).
6. J. H. E. Cartwright, O. Piro, I. Tuval, *Proc. Natl. Acad. Sci. U.S.A.* **101**, 7234 (2004).
7. Q. Wang, J. Pan, W. J. Snell, *Cell* **125**, 549 (2006).
8. C. A. Solari, S. Ganguly, J. O. Kessler, R. E. Michod, R. E. Goldstein, *Proc. Natl. Acad. Sci. U.S.A.* **103**, 1353 (2006).
9. S. Gueron, K. Levit-Gurevich, *Proc. Natl. Acad. Sci. U.S.A.* **96**, 12240 (1999).
10. B. Guirao, J. F. Joanny, *Biophys. J.* **92**, 1900 (2007).
11. A. Vilfan, F. Julicher, *Phys. Rev. Lett.* **96**, 058102 (2006).
12. T. Niedermayer, B. Eckhardt, P. Lenz, *Chaos* **18**, 037128 (2008).
13. H. C. Berg, D. A. Brown, *Nature* **239**, 500 (1972).
14. H. C. Berg, *Random Walks in Biology* (Princeton Univ. Press, Princeton, NJ, 1983).
15. C. Ainsworth, *Nature* **448**, 638 (2007).
16. *The Chlamydomonas Sourcebook*, E. H. Harris, D. Stern, G. Witman, Eds. (Elsevier, Oxford, ed. 2, 2009).
17. U. Rüffer, W. Nultsch, *Cell Motil.* **7**, 87 (1987).
18. U. Rüffer, W. Nultsch, *Cell Motil.* **41**, 297 (1998).
19. K. Josef, J. Saranak, K. W. Foster, *Cell Motil. Cytoskeleton* **61**, 83 (2005).
20. N. Okita, N. Isogai, M. Hirono, R. Kamiya, K. Yoshimura, *J. Cell Sci.* **118**, 529 (2005).
21. V. A. Vladimirov, M. S. C. Wu, T. J. Pedley, P. V. Denissenko, S. G. Zakhidova, *J. Exp. Biol.* **207**, 1203 (2004).
22. N. A. Hill, D.-P. Häder, *J. Theor. Biol.* **186**, 503 (1997).
23. P. Hegemann, B. Bruck, *Cell Motil.* **14**, 501 (1989).
24. Materials and methods are available as supporting material on *Science* Online.
25. A. Pikovsky, M. Rosenblum, J. Kurths, *Synchronization. A Universal Concept in Nonlinear Science* (Cambridge Univ. Press, Cambridge, 2001).
26. K. Drescher, K. Leptos, R. E. Goldstein, *Rev. Sci. Instrum.* **80**, 014301 (2009).

27. We thank K. Leptos, T. J. Pedley, C. A. Solari, K. Visscher, A. Nedelcu, D. Page-Croft, T. Parkin, and N. Price and acknowledge support from the Marie-Curie Program (M.P.), the Human Frontiers Science Program (I.T.), the Leverhulme Trust (J.P.G.), the Biotechnology and Biological Sciences Research Council, the Engineering and Physical Sciences Research Council, the U.S. Department of Energy, and the Schlumberger Chair Fund.

Supporting Online Material

www.sciencemag.org/cgi/content/full/325/5939/487/DC1
Materials and Methods
Figs. S1 to S3
References

23 February 2009; accepted 2 June 2009
10.1126/science.1172667

Translocator Protein (18 kD) as Target for Anxiolytics Without Benzodiazepine-Like Side Effects

Rainer Rupprecht,[1,2]* Gerhard Rammes,[2,3] Daniela Eser,[1] Thomas C. Baghai,[1] Cornelius Schüle,[1] Caroline Nothdurfter,[1,2] Thomas Troxler,[4] Conrad Gentsch,[4] Hans O. Kalkman,[4] Frederique Chaperon,[4] Veska Uzunov,[4] Kevin H. McAllister,[4] Valerie Bertaina-Anglade,[5] Christophe Drieu La Rochelle,[5] Dietrich Tuerck,[6] Annette Floesser,[4] Beate Kiese,[7] Michael Schumacher,[8] Rainer Landgraf,[2] Florian Holsboer,[2] Klaus Kucher[4]

Most antianxiety drugs (anxiolytics) work by modulating neurotransmitters in the brain. Benzodiazepines are fast and effective anxiolytic drugs; however, their long-term use is limited by the development of tolerance and withdrawal symptoms. Ligands of the translocator protein [18 kilodaltons (kD)] may promote the synthesis of endogenous neurosteroids, which also exert anxiolytic effects in animal models. Here, we found that the translocator protein (18 kD) ligand XBD173 enhanced γ-aminobutyric acid–mediated neurotransmission and counteracted induced panic attacks in rodents in the absence of sedation and tolerance development. XBD173 also exerted antipanic activity in humans and, in contrast to benzodiazepines, did not cause sedation or withdrawal symptoms. Thus, translocator protein (18 kD) ligands are promising candidates for fast-acting anxiolytic drugs with less severe side effects than benzodiazepines.

Anxiety disorders are highly prevalent disabling disorders (*1*) that frequently turn into chronic clinical conditions (*2*). Benzodiazepines such as diazepam are fast-acting and effective antianxiety agents (*3*–*5*) and the most commonly prescribed anxiolytics. However, their side effects such as sedation and, following chronic administration, development of tolerance, consecutive abuse liability, and withdrawal symptoms render their use problematic in the long-term treatment of anxiety disorders (*2*–*4*). Currently, antidepressants such as selective serotonin reuptake inhibitors are first-line treatment for most anxiety disorders. However, their anxiolytic effects occur only after several weeks of treatment (*2*–*4*). Thus, there is need for anxiolytic agents that retain the rapid anxiolytic potential of benzodiazepines but lack their unfavorable side effects.

Neurosteroids are synthesized from cholesterol or steroidal precursors and modulate neurotransmitter receptors (*6*–*8*). Ring A–reduced neurosteroids are endogenous metabolites of the hormone progesterone and potent positive allosteric modulators of γ-aminobutyric acid type A ($GABA_A$) receptors, which mediate the effects of the inhibitory neurotransmitter GABA in the mammalian nervous system (*6*–*8*). They exert pronounced anxiolytic effects in animal models (*9*–*11*), and their concentrations are reduced

www.sciencemag.org/cgi/content/full/325/5939/487/DC1

Supporting Online Material for

Chlamydomonas Swims with Two "Gears" in a Eukaryotic Version of Run-and-Tumble Locomotion

Marco Polin, Idan Tuval, Knut Drescher, J. P. Gollub, Raymond E. Goldstein*

*To whom correspondence should be addressed. E-mail: R.E.Goldstein@damtp.cam.ac.uk

Published 24 July 2009, *Science* **325**, 487 (2009)
DOI: 10.1126/science.1172667

This PDF file includes:

Supporting Online Material

Materials and methods

Culturing of algae

Experiments were conducted on *Chlamydomonas reinhardtii* (UTEX 89 (*S1*)), grown axenically in standard *Volvox* medium (SVM (*S2*)) with sterile air bubbling, in diurnal growth chambers (Binder KBW400, Tuttlingen, Germany) set to a daily cycle of $16\,\mathrm{h}$ in cool white light ($\sim 4000\,\mathrm{lux}$) at 28° C, and $8\,\mathrm{h}$ in the dark at 26° C. In all experiments, the algae were harvested during the exponential growth phase ($\lesssim 10^6$ cells/ml), to guarantee high uniformity and health of the population.

Macroscopic diffusion experiment

For the macroscopic diffusion experiment, we used the horizontal view camera of the 3D tracking setup (described below) in darkfield. Newly harvested suspensions of *C. reinhardtii* were transferred to $1.5\,\mathrm{ml}$ disposable Plastibrand UV-cuvettes (Brand GmbH, Wertheim, Germany), where they filled a volume of $\sim 20 \times 12.2 \times 4\,\mathrm{mm}$. Each sample was then sealed with an expanded polystyrene foam cork, and centrifuged at $350\,\mathrm{g}$ for $2.5\,\mathrm{min}$, causing the sedimentation of the suspended algae. After centrifugation, the samples were transferred to the tracking setup and the upward spreading of the cells' density profile was recorded at $10\,\mathrm{fps}$ for $1-2\,\mathrm{min}$. In all experiments, recording started within the first $20\,\mathrm{s}$ after centrifugation. The samples were illuminated by a narrowband LED with an emission peak centered at $655\,\mathrm{nm}$, and a bandwidth of $21\,\mathrm{nm}$. *C. reinhardtii* is insensitive to these wavelengths (*S3, S4*), so phototactic reorientations do not occur. After each experiment, we homogenized the suspension by vortexing and estimated the average cell density with a Neubauer haemocytometer (Fisher Scientific, Pittsburgh,

PA). All experiments were done at average densities smaller than 2.7×10^6 cells/ml to minimize cell-cell interactions.

We also examined the possible influence of thermal convection by recording the motion of a suspension of $1\,\mu$m polystyrene beads (F8823, Invitrogen, Carlsbad, CA) in the same cuvette and under the same observation conditions as the previous experiments. The motion of the tracer particles was analyzed with an open source Matlab PIV toolbox (MatPIV, http://www.math.uio.no/∼jks/matpiv/) and found to be below $13\,\mu$m/s.

Flagellar dynamics experiment

Sample cells were constructed by gluing two strips of $3\,$mm thick expanded polystyrene foam between two microscope coverslips. Two sides of the cell were left open to allow access. For each experiment a new sample cell was filled with fresh sterile filter-cleaned SVM at room temperature. A small number of *C. reinhardtii* cells were harvested from the culturing flask during the light cycle, and immediately transferred to the sample cell. Observations started $30\,$min after transfer to allow for acclimatization. Individual cells were held at the end of a micropipette with a tip opening of $2 - 4\,\mu$m, prepared with a commerical pipette puller (P-97, Sutter Instrument Co., Novato, CA) and reshaped with a microforge (DMF1000, World Precision Instruments, Sarasota, FL). Pipettes were held in a motorized micromanipulator under joystick control (PatchStar, Scientifica, Uckfield, UK) by means of pipette holders (World Precision Instruments) mounted on small custom made rotation stages. This arrangement allowed free rotation around the pipette axis, which was crucial for reorienting the cells and achieving optimal visualization of their flagella. Cells were held by gentle suction, controlled by a gas-tight syringe fitted with micrometer control (Manual Injector, Sutter). Imaging was done under brightfield illumination on a custom-built stage mounted on a Nikon TE2000-U inverted microscope with a Nikon Plan Fluor ELWD $40\times$ objective (NA 0.6). The light from the microscope's

halogen lamp was filtered through a long pass interference filter with a 10 nm transition width between 0.001% and 80% transmittance, centered at 620 nm (Knight Optical, Harrietsham, UK). These wavelengths were selected to avoid any phototactic response (*S3, S4*). Videos were acquired at 500 fps with a high-speed video camera (Phantom V5.1, Vision Research, Wayne, NJ) with 4 Gb of on-board memory, mounted on the microscope's camera port, and transferred to disk afterwards.

Experiment on rotation of uniflagellated cells

During periods of asynchrony one flagellum beats faster than the other, a pattern that should naturally lead to turns in the swimming trajectory. We reasoned that the turning rate induced by the faster flagellum could be estimated from the turning rate of a cell with a single flagellum. PVC O-rings 2 mm thick and 1 cm in diameter were fixed on the surface of microscope coverslips coated with a $\sim 200\,\mu$m thick layer of Polydimethylsiloxane (PDMS) (Sylgard 184, Dow Corning Ltd, Coventry, UK) and sealed from outside with additional PDMS to create a circular chamber open from the top. The chambers were then cured at 60° C for 90 min, plasma etched with dry air for 30 s (Femto System, Diener Electronic, Germany) and left overnight immersed in 5% bovine serum albumin (BSA) in phosphate-buffered saline solution at 4° C. This treatment minimizes sticking of *C. reinhardtii* to the bottom of the chamber (*S5*). Before each experiment, a new chamber was taken from the BSA solution, carefully washed with fresh SVM, then filled with fresh SVM at room temperature, and placed on the stage of a Nikon TE2000-U inverted microscope. For each experiment, a small sample was harvested from the *C. reinhardtii* culturing flask and gently sheared in a borosilicate Dounce homogenizer (Fisher) to create a sub-population of uniflagellated algae. A small volume from the sheared suspension was then transferred to the observation chamber. The uniflagellated cells are unable to swim and therefore sink to the bottom of the cell, where they start rotating in place under the action of

their only flagellum. Each batch was observed for no longer than 15 min after homogenization. We recorded the rotation of 8 randomly chosen cells for 50 s each. All observations were done under the same brightfield conditions, with the same objective, and with the same high-speed camera used for the flagellar dynamics experiment.

Three-dimensional tracking experiment

To track *C. reinhardtii*, in three dimensions, a custom-built dual view apparatus was employed (*S6*). Previous studies in which *Chlamydomonas* has been tracked were done in 2D (*S7, S8, S9*) or with a 3D moving stage tracking microscope (*S10*). The cells were imaged from two orthogonal directions by two identical assemblies, each consisting of a long working distance microscope (InfiniVar CFM-2/S, Infinity Photo-Optical, Boulder, CO) directly attached to a grayscale FireWire CCD camera (Pike F145B, Allied Vision Technologies, Stadtroda, Germany). The sample was illuminated in darkfield by red annular LED arrays (LFR-100-R, CCS Inc., Kyoto, Japan, peak emission at 655 nm, bandwidth 21 nm). Images were acquired synchronously from both cameras with custom Labview (National Instruments, Austin, TX) routines at 20 fps and at a magnification of $0.63\times$. A set of 2D tracks was then computed for the image sequences acquired by each camera. As the two cameras had one common axis, 3D tracks could be reconstructed by locking together two 2D tracks which overlapped in time and had a strongly correlated trajectory along the common axis. This method allowed 10 - 100 *C. reinhardtii* cells to be tracked in one image sequence with a spatial precision better than $3\,\mu$m at each time point. The sample, a $1 \times 1 \times 4$ cm quartz cuvette (111-10-40, Hellma, Müllheim, Germany), was filled with *C. reinhardtii* suspended in SVM (cleaned by filtration through a $0.2\,\mu$m filter) at a concentration of $\sim 10^2$ cells/ml. Measurements began 15 min after the sample was placed in the centre of a stirred water bath at 22° C, as control studies with $10\,\mu$m polystyrene microspheres (C37259, Invitrogen) showed that thermal convection ceased ~ 10 min after the sample was

placed in the water bath. The apparatus was calibrated and tested as described by Drescher et al. (*S6*).

Data analysis

All analyses were done with customized Matlab routines.

Flagellar dynamics experiment

We analyzed 24 different cells and gathered individual time series lasting typically 3 min each. Each movie was processed by local background subtraction followed by light smoothing to enhance the contrast of the flagella. The cell dynamics was quantified by monitoring the passage of each flagellum across a small interrogation region on either side of the cell body (Fig. 2A), and representing the resultant oscillatory signals of the left (L) and right (R) flagella as $X_{L,R}(t) = \Gamma_{L,R}(t)\sin(2\pi\theta_{L,R}(t))$, where Γ is the amplitude and θ is the phase, normalized to advance by 1 per cycle. Unfortunately we could not determine the correspondence between L/R and *cis*/*trans* flagella. This correlation could be important to connect our findings to phototaxis, where intrinsic differences between *cis* and *trans* flagella are thought to play a major role (*S11*), but it does not influence our results and was not pursued further.

For the issue of synchronization, we focus attention on the phase difference $\Delta(t) = \theta_L(t) - \theta_R(t)$. We define the instantaneous beating rate of the flagellum i as $\nu_i = d\theta_i/dt$, and thus in synchronous beating Δ is a constant, whereas asynchronous dynamics appears as a "drifting" phase with temporal slope $d\Delta/dt = \nu_L - \nu_R$. We analyzed separately the dynamics of $\Delta(t)$ during periods of synchrony and during periods of drift. While the detailed microscopic equations of motion of beating flagella have been the subject of extensive research (*S12, S13*), we focus instead on how the simplest mathematical model of noisy coupled oscillators can capture the basic phenomenology of the observed time series, and give insights into the underlying bio-

chemical processes. Under general conditions the dynamics of weakly nonlinear self-sustained oscillators obey a universal equation (*S14*) dictacted by symmetries. Modifying this to include noise of the oscillators leads to a stochastic ordinary differential equation for the phase difference (*S14*)

$$\frac{d\Delta}{dt} \;=\; \delta\nu - 2\pi\epsilon \sin\left(2\pi\Delta\right) + \xi(t)\;, \tag{1}$$

where $\delta\nu = \nu_L - \nu_R$ is the difference between the intrinsic frequencies of the two flagella, ϵ the coupling strength, and ξ is Gaussian white noise with $\langle\xi(t)\rangle = 0$ and correlation $\langle\xi(t)\xi(t')\rangle = 2\,T_{\text{eff}}\,\delta(t-t')$. Here T_{eff} is an effective "temperature" by analogy with systems in thermal equilibrium. Without noise, Eq. 1 has been derived from the low Reynolds number hydrodynamic interaction between two idealized flagella (*S15*). This derivation yields a rough estimate ϵ_m for the hydrodynamic contribution to the coupling as a function of the separation of the flagella. In the present case $\epsilon_m = 0.006 \times \bar{\nu}$, where $\bar{\nu} = 50\,\text{Hz}$ is the average flagellar beating frequency. At a heuristic level, Eq. 1 also describes the noise-driven motion of a massless particle on a "tilted washboard" potential, a rich problem with broad applicability (*S16, S17*). Applied to *C. reinhardtii*, this model describes periods of synchrony as localized fluctuations around a single metastable minimum of the effective potential. The noise can induce occasional hopping between metastable states, representing an extra beat of one of the flagella (a "phase slip"). The intrinsic frequency difference $\delta\nu$ corresponds to a global tilt in the washboard potential, which favors slips in one direction.

During synchronous periods, Eq. 1 predicts that fluctuations of $\Delta(t)$ should have an exponentially decaying autocorrelation function, $R(t) = R_0\,\mathrm{e}^{-t/\tau_{\text{ac}}}$, which is indeed observed experimentally (Fig. S1). If the coupling strength $2\pi\epsilon$ is sufficiently larger than the bias $\delta\nu$, the

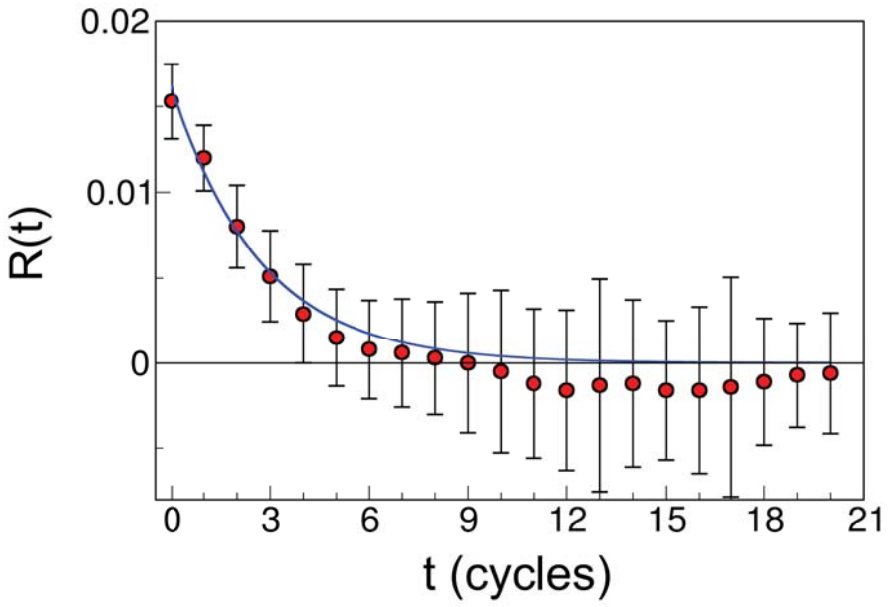

Figure S1: Average autocorrelation function $R(t)$ in the synchronized state for one experiment, showing exponential decay with a characteristic time of $\simeq 2$ cycles. Errorbars represent the standard deviations of the distributions used to calculate the averages.

parameters of the autocorrelation function can be expressed as

$$R_0 = \tau_{\text{ac}}\, T_{\text{eff}} \quad ; \quad \tau_{\text{ac}} = \frac{1}{2\pi\sqrt{(2\pi\epsilon)^2 - \delta\nu^2}}. \tag{2}$$

Following Eq. 1, we can also express the ratio p_+/p_- between the probabilities of forward and backward slips as

$$p_+/p_- = \exp(\delta\nu/T_{\text{eff}}). \tag{3}$$

Experimentally, this quantity can be estimated as the ratio between the number of positive and negative slips. We used Eqs. 2 and 3 to derive the parameters representing the synchronous dynamics of each experiment. The results ($2\pi\epsilon \simeq 10\,\delta\nu$) justify the use of the approximate relations in Eq. 2. These parameters are also consistent with independent observables like the

small interflagellar phase lag during synchrony reported in previous studies ($\simeq 1/11$th of a cycle, (*S18*)), and the average time between successive slips. During drift periods $\Delta(t)$ depends linearly on time with a slope given by the bias, $\delta\nu$. Fluctuations around this linear behavior provide a direct measurement of the effective temperature T_{eff}. In this regime, the coupling strength is much smaller than the bias, and cannot be estimated.

For the purposes of presentation, the fitted parameters $\delta\nu$, ϵ, and T_{eff} are rescaled by the mean observed flagellar beating frequency $\bar{\nu}$. For the synchronous intervals, the distribution of the measured coupling parameter $\epsilon/\bar{\nu}$ (Fig. 3A) shows a well-defined peak at a value of 0.0076, which compares very well with the rough estimate $\epsilon_m/\bar{\nu} = 0.006$ given by the idealized flagellar model with hydrodynamic coupling (*S15*). The synchronous and asynchronous states cluster into two distinct regions in the parameter space $(\delta\nu, T_{\text{eff}})$ (Fig. 3B). Synchronous states have $\delta\nu/\bar{\nu} \simeq 0.001 - 0.01$, while asynchronous states display $\delta\nu/\bar{\nu} \simeq 0.1 - 0.4$. The latter is in agreement with the asynchronous characteristics reported in earlier work (*S18, S19, S20*). We never observed any cell whose frequency difference falls in between these two clusters.

Experiment on rotation of uniflagellated cells

Recorded movies were processed as reported in the previous section. We measured the rotation speed of the cell bodies using the signal from a single interrogation region inside the body's image. At the same time, the beating frequency of the flagellum was measured from its passage across a ring-shaped interrogation area around the cell body. As this estimate neglects the drag produced by the second flagellum it provides an upper bound on the possible angular speeds. The ratio between the body's mean angular velocity and the beating frequency of the flagellum gives the angular deviation per beat. From 8 cells we obtain an average rotation rate $\phi = 0.43 \pm 0.06$ rad/beat, consistent with an earlier observation of cell rotation by a single active flagellum after a photoshock response (*S21*). In low Reynolds number flow, this value is

independent of flagellar beating frequency and depends only on the geometry of the beat. From the observed difference in flagellar beating frequencies during drifts, $\delta\nu = 5-15$ Hz, we obtain the two-dimensional angular speed $\Omega_{2D} = \phi\,\delta\nu \simeq 2-6$ rad/s.

This simple derivation neglects the influence of the nearby wall on the cell body's drag coefficient. However, since the cell's angular velocity is perpendicular to the wall, this effect is negligible (*S22*), and the previous measurements give a sound estimate of the angular velocity Ω_{2D} that a cell would have during drift periods, if its motion was planar. This is an upper bound, as the helical progression of free swimming cells tends to average out the effect of a constant frequency difference between the two flagella. A more accurate estimate can be derived if we model a cell freely swimming in the laboratory frame of reference, as simply spinning at a constant speed ω around its own body axis. During periods of drift, this axis rotates at an angular speed Ω_{2D} around an axis fixed in the body frame. The resulting maximum angular speed of the body axis in the laboratory frame, Ω_{3D}, can be readily calculated. For $\omega = 2\pi - 4\pi$ rad/s (*S18*) and $\Omega_{2D} = 2-6$ rad/s, we obtain $\Omega_{3D} = 0.1 - 0.7 \times \Omega_{2D} \simeq 0.8 - 2.4$ rad/s compatible with the range of maximum angular speeds obtained from 3D tracks.

Tracking experiment

From the three-dimensional tracks, the angular speed Ω between timesteps i and $i+1$ was computed by multiplying the frame rate (20 fps) by the angle between the normalized velocity vectors $\hat{\mathbf{v}}_i$, and $\hat{\mathbf{v}}_{i+1}$. To reduce noise, and the effect of the swimming helix, the velocity vector $\hat{\mathbf{v}}_j$ was computed by fitting a second order polynomial to time series of x, y, and z that contain 51 positions (from $j-25$ to $j+25$) and differentiating this fit at time j. This procedure yields a time series $\Omega(t)$ that retaines a background signal $\lesssim 0.3$ rad/s, and occasional large peaks. We identified peaks to be "large peaks", when the local maximum of the peak, Ω_{peak}, was larger than the preceding and succeding local minima by 0.5 rad/s. This threshold was verified by

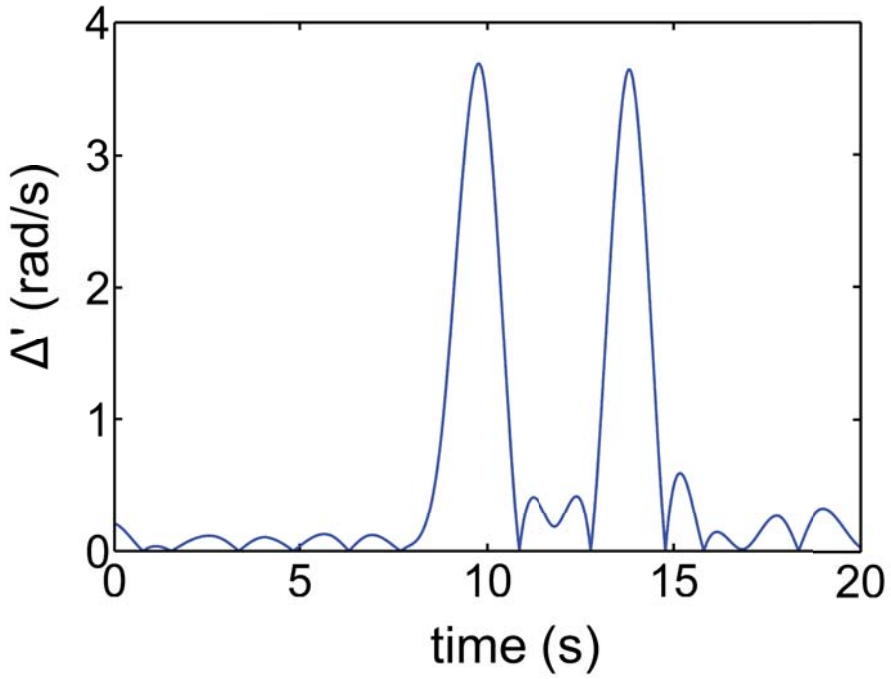

Figure S2: Time derivative $\Delta'(t)$ of the smoothed interflagellar phase difference shows two clear peaks corresponding to two periods of phase drift. The width of the peaks measures the duration of the drifts.

checking that the large peaks in $\Omega(t)$ correspond to obvious large-angle turns in the 3D tracks. We estimated the duration t_{turn} of these peaks by fitting a Gaussian $\sim \exp(-2\,t^2/t_{\text{turn}}^2)$. This leads to an esimate of the turning angle $\alpha = t_{\text{turn}}\,\Omega_{\text{peak}}$.

A similar procedure was used to estimate the duration of drift periods from the long time series of interflagellar phase difference $\Delta(t)$. To reduce noise, and the effect of the short slips, the time derivative $\Delta'(t)$ of the signal was computed by fitting a second order polynomial to the time serie of $\Delta(t)$ that contain 500 frames (from $t-250$ to $t+250$) and differentiating this fit at time t. This procedure yields a time series $\Delta'(t)$ that retaines a background signal $\lesssim 0.5$ rad/s, and occasional large peaks (Fig. S2). We identified peaks to be "large peaks", when the local maximum of the peak, Δ'_{peak}, was larger than the preceding and succeding local minima by

1 rad/s. This threshold was verified by checking that the large peaks in $\Delta'(t)$ correspond to obvious drifts in the interflagellar phase difference. Again, we estimated the duration t_{drift} of these peaks by fitting a Gaussian $\sim \exp(-2\,t^2/t^2_{\text{drift}})$. All slips (jumps of ± 1 in the time series for $\Delta(t)$) in each experiment were identified and averaged and the time derivative $\Delta'(t)$ of the averaged signal was then computed. A Gaussian fit $\sim \exp(-2\,t^2/t^2_{\text{slip}})$ to the obtained peak gave then an estimate for the slips duration t_{slip}. The "free flight time" τ is defined as the time between successive large peaks in $\Omega(t)$.

Diffusion experiment

For each movie the intensity distribution inside the cuvette was integrated along the cuvette width to give the raw signal $I_{\text{raw}}(x,t)$, where $x \in [0, L]$ is the coordinate along the cuvette length, and $t \in [0, T]$ is the elapsed time from the beginning of the movie. We used $I_{\text{raw}}(x, 0)$ to estimate the background intensity distribution, which was then subtracted from the raw signal to give the real intensity distribution $I(x,t)$. Independent experiments established that this signal is proportional to the local cells' concentration, at least for concentrations up to $\sim 2 \times 10^6$ cells/ml. The initial intensity profile is typically localized in the bottom 10% of the cuvette (2 mm, with the peak at 1 mm). During an experiment it spreads upwards, until at time T it just reaches the upper limit of the region of interest. Given l such that $I(l, T) = 0.5 \times \max(I(x, T))$, we estimated intensity gradients and fluxes at a uniformly spaced set of points for $x \in [l, L]$ and $t \in [0, T]$. The gradients were calculated from a local linear interpolation to the intensity profile. The fluxes were estimated from the time changes in the integrated intensity above the point of interest. The linear relation between measured fluxes and gradients (Fig. 1A) is a clear verification of Fick's law and allows a direct determination of the diffusion constant for an isolated individual: $D_{\text{exp}} = (0.68 \pm 0.11) \times 10^{-3}$ cm^2/s (from $n = 8$ population trials).

From the initial position of the peak, the spread of the intensity distribution at time T,

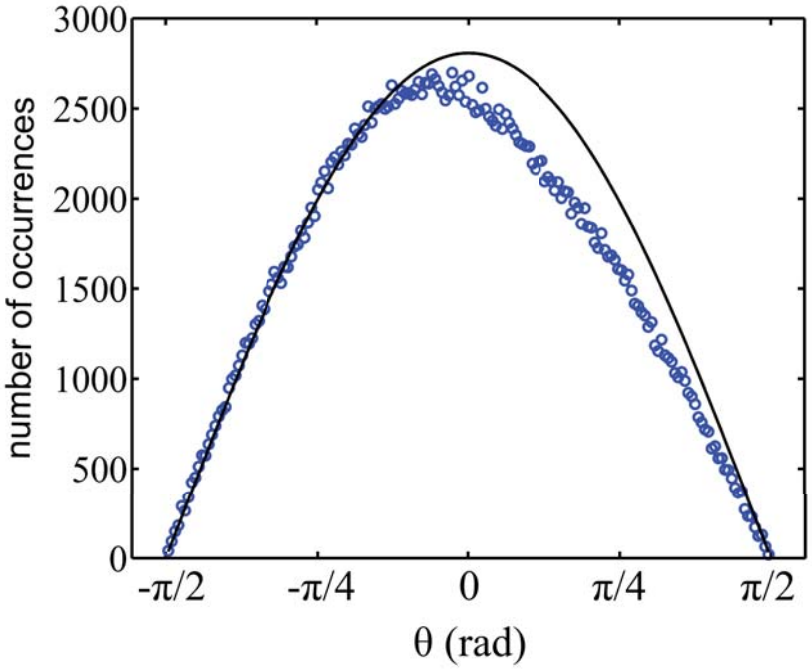

Figure S3: Comparing the distribution of swimming angles (rad) over the horizontal plane from 3D tracks (circles), and the expected distribution for isotropic swimming (solid line) shows a net preference for upward swimming (negative angles).

and the average cell density (measured a posteriori with the cell counter), we can estimate the maximum value of the cell concentration in the selected range ($x \in [l, L]$ and $t \in [0, T]$). The estimate falls below 10^6 cells/ml for all experiments. This concentration is well below that at which close cell-cell encounters may occur more frequently than once per mean flight time, which can be estimated as $n = 1/(\pi\, u\tau d^2) \simeq 3 \times 10^6$ cells/ml, where $u = 100\,\mu$m/s is the mean swimming speed, $\tau \simeq 10\,$s is the mean free flight time, and $d = 10\,\mu$m is the cell's diameter.

C. reinhardtii cells often show a slight preference for upward swimming (negative gravitaxis (*S23*)), which causes a net drift v_d in the upward direction. This is true also in the present case (Fig. S3). Analysis of the recorded 3D trajectories gives $v_d = 5 - 10\,\mu$m/s, in line with previous measurements (*S24*). This drift will skew our estimate of the diffusion coefficient as

$D_{\text{exp}}/D \simeq (1 + v_d\ \delta t/\delta x)$, where δt and δx are the characteristic time and distance at which intensity fluxes and gradients were measured. For $\delta t \sim 100\,\text{s}$ and $\delta x \sim 0.5 - 1\,\text{cm}$ we predict that D_{exp} will slightly overestimate the diffusion constant: $D_{\text{exp}} \simeq 1.1\,D$. Furthermore, slight variations in behavior among different individuals in a whole population will result in slightly different diffusivities. The method we use to estimate the population's average diffusion constant will bias the estimate again towards higher values, since the individuals with higher diffusivity will tend to be overrepresented in the analyzed range. This is also a weak effect because, for example, a normally distributed ensemble of diffusion constants with a standard deviation twice the mean (and truncated to non-negative diffusivities), would give an estimated average diffusion constant only 20% higher than the real mean. The real distribution of diffusivities is certainly narrower than this example, and will give an even smaller bias. Taken together, these two effects may contribute to the small discrepancy between the measured and estimated diffusion constants.

References and Notes

S1. UTEX is the algal culture collection of the University of Texas at Austin.

S2. D.L. Kirk and M.M. Kirk, *Dev. Biol.* **96**, 493 (1983).

S3. O.A. Sineshchenkov, K.-H. Jung, and J.L. Spudich, *Proc. Natl. Acad. Sci. USA* **99**, 8689 (2002).

S4. P. Lariguet and C. Dunand, *J. Mol. Evol.* **61**, 559 (2005).

S5. D.B. Weibel, P. Garstecki, D. Ryan, W.R. DiLuzio, M.Mayer, J.E. Seto, and G.M. Whitesides, *Proc. Natl. Acad. Sci. USA* **102**, 11963 (2005).

S6. K. Drescher, K. Leptos, and R.E. Goldstein, *Rev. Sci. Instrum.* **80**, 014301 (2009).

S7. P. Hegemann and B. Bruck, *Cell. Mot.* **14**, 501 (1989).

S8. V.A. Vladimirov, M.S.C. Wu, T.J. Pedley, P.V. Denissenko, and S.G. Zakhidova, *J. Exp. Biol.* **207**, 1203 (2004).

S9. N.A. Hill and D.-P. Häder, *J. Theor. Biol.* **186**, 503 (1997).

S10. H.C. Berg, *Adv. Opt. Elect. Microsc.* **7**, 1 (1978).

S11. U. Rüffer and W. Nultsch, *Cell. Mot.* **18**, 269 (1991).

S12. C. Brennen and H. Winet, *Ann. Rev. Fluid Mech.* **9**, 339 (1977).

S13. I. H. Riedel-Kruse, A. Hilfinger, J. Howard, and F. Jülicher, *HFSP J.* **1**, 192 (2007).

S14. A. Pikovsky, M. Rosenblum, and J. Kurths, *Synchronization. A universal concept in nonlinear science* (Cambridge University Press, Cambridge, 2001).

S15. T. Niedermayer, B. Eckhardt, and P. Lenz, *Chaos* **18**, 037128 (2008).

S16. P. Hänggi, P. Talkner, and M. Borkovec, *Rev. Mod. Phys.* **62**, 251 (1990).

S17. P. Reimann, C. van den Broeck, H. Linke, P. Hänggi, J.M. Rubi, and A. Pérez-Madrid, *Phys. Rev. E* **65**, 031104 (2002).

S18. U. Rüffer and W. Nultsch, *Cell. Mot.* **5**, 251 (1985).

S19. R. Kamiya and E. Hasegawa, *Exp. Cell Res.* **173**, 299 (1987).

S20. N. Okita, N. Isogai, M. Hirono, R. Kamiya, and K. Yoshimura, *J. Cell Sci.* **118**, 529 (2005).

S21. U. Rüffer and W. Nultsch, *Cell. Mot.* **15**, 162 (1990).

S22. G.B. Jeffery, *Proc. London Math. Soc.* **22** (14), 327 (1915).

S23. A. M. Roberts, *Biol. Bull.* **210**, 78 (2006).

S24. B. Bean, *J. Protozool.* **24**, 394 (1977).